Theory of Optical Generation and Detection of Propagating Magnons in an Antiferromagnet

R.A. Leenders, R.V. Mikhaylovskiy*

Department of Physics, Lancaster University, Bailrigg, Lancaster LA1 4YW, UK

We report a theory of optical generation and detection of the propagating spin waves in antiferromagnetic materials relevant for the ultrafast pump-probe experiments. We derive and solve the equations of motion for antiferromagnetic spins in response to the light-induced effective magnetic field in the linear regime. Different forms of the excitation and the properties of the generated spin waves are analysed. We theoretically show the selective detection of the spin waves by the magneto-optical Kerr effect. The developed formalism is readily applicable to inform future experiments on antiferromagnetic opto-magnonics.

* r.mikhaylovskiy@lancaster.ac.uk

I: Introduction

The quest for the minimally dissipative processing of information has led to the search for an information carrier alternative to the traditional electric currents, suffering from ever growing energy losses[1-3]. In this way, the waves of the propagating spin precession, i.e. spin waves, in magnetically ordered materials have been identified as new means to carry information[4,5]. The spin waves, of which the quanta are also known as magnons, are magnetic excitations, which do not involve transport of charge and hence are free from Ohmic losses. Thus, in the last years a huge progress has been made in the area of magnonics, i.e. the study of spin waves and their practical applications[6,7]. However, most of the demonstrations and discoveries in this field are restricted to ferromagnetic materials with relatively low clock-rates (~ GHz).

The use of antiferromagnetic materials with antiparallel spin alignment instead of conventional ferromagnets can potentially push operation frequencies into the THz regime and attain higher spin wave velocities[8,9]. However, until recently the lack of straightforward mechanisms to generate the spin excitations with such high frequencies was a main impediment for magnonics in antiferromagnets. The solution came with an advent of ultrafast laser technologies. For instance, the femtosecond laser pulses were shown to drive antiferromagnetic resonances both thermally[10] and non-thermally[11]. In the former case the laser pulse affects the temperature dependent magnetic anisotropy and equilibrium orientation of spins, thereby exerting a displacive torque on the spins[12,13]. In the latter case the action of the laser pulse can be described as producing an impulsive effective magnetic field (and hence torque), acting on spins[11,14]. The microscopic mechanism for this effective magnetic field is impulsive stimulated Raman scattering[15,16]. Another way to directly drive antiferromagnetic spins is to use transient THz pulses. The THz magnetic field directly couples to magnetic excitations in the linear regime[17,18], while the electric field can modify the magnetic anisotropy in a nonlinear manner[19]. Moreover, the femtosecond optical pulses allow for time resolved magneto-optical detection of sub-picosecond spin dynamics using magneto-optical effects[20-22]. In addition, coherent antiferromagnetic oscillations emit THz signals, which can also be detected using THz time-domain spectroscopy methods[23-29].

Yet, despite all these achievements, the optical generation of the coherent propagating spin waves has remained a major challenge. The main problem is the huge mismatch between the wavelength and minimal spot size of the electro-magnetic radiation at optical (~ 100 nm) or THz (~ 100 μm) frequencies and the wavelength of spin waves in antiferromagnets (~ 10 nm).

Therefore, in the typical experiments only quasi-uniform precession modes are excited, while the practical applications call for propagating spin waves. In principle, the propagation can be achieved in the strong coupling regime between the electro-magnetic THz pulses and the antiferromagnetic modes[30]. In such a case the hybrid magnon-polariton modes are formed, propagating with the speed of light[31]. However, the wavelength of the magnon-polaritons lies in ~ 10 μm scale that inhibits miniaturization down to nanoscale. At the same time, excitation of the standing spin waves[32-34] or so-called two-magnon modes[35] can achieve nanoscale at the expense of zero group-velocities and lack of the desired propagation. As a result, recent experimental realizations of spin wave transport in antiferromagnets were limited to either diffusive propagation of incoherent magnons[36-38] or evanescent modes[39].

In ferromagnets, in which magneto-static spin waves have microscale wavelengths, the propagating magnons can be excited by strongly focused laser pulses[40-42]. If the excitation torque is confined to a region with a size smaller than the magnon wavelength, this magnon will propagate away from the excitation spot. In an antiferromagnet with nanoscale spin waves, the simple focusing of a laser pulse cannot work. Only recently the excitation confinement was achieved across the sample thickness in antiferromagnetic ferrite $DyFeO_3$ by pumping it with a laser pulse with photon energy in the regime of strong absorption[43]. The laser pulse penetration depth was about 50 nm that allowed the generation of the spin waves propagating away from the sample face with the wavelengths of this order. The excited spin waves also acted as an effective diffraction grating for the reflected probe pulse, enabling their selective detection. Taking inspiration from this pioneering experimental study, in this work we present a thorough theoretical analysis of the optical generation and detection of the antiferromagnetic magnons in pump-probe experiments.

The paper is organized as follows. In Section II we introduce the basic mathematical formalism, describing the excitation of magnons by laser pulses in an antiferromagnet. In Section III we apply this general formalism to various experimental configurations, calculating the laser-driven spin dynamics in the cases of impulsive and displacive excitations and different boundary conditions. We compare the results of most simplistic approximations such as reducing the effective magnetic field pulse to a Delta-function and the more complete models of propagating Gaussian pulses. We also study the role of material parameters like laser penetration depth, spin pinning, spin wave velocity and damping. Section IV exposes the theory describing the detection of the spin waves by means of the magneto-optical Kerr effect, while

Section V demonstrates the selective detection observed in the experiment. We draw conclusions in Section VI.

II. Model and Mathematical Formalism

A schematic illustration of the modelled system is depicted in Figure 1. We consider a canted antiferromagnet (for generality, our theory is also applicable for zero canting), consisting of two sublattices containing magnetizations $\mathbf{M}_1$ and $\mathbf{M}_2$. In our model, we assume that the antiferromagnetic vector $\mathbf{L}=\mathbf{M}_1-\mathbf{M}_2$ is oriented along the *x*-axis, and the ferromagnetic vector $\mathbf{M}=\mathbf{M}_1+\mathbf{M}_2$ is oriented along the *z*-axis. When an antiferromagnet is excited by a laser pulse, the excitation leads to a change in magnetic parameters.[29] We take this into our model by considering that the laser pulse acts as an effective magnetic field on the spin system.[11] The effective field may arise from the light-induced magnetic anisotropy[44,45], exchange interaction,[46,47] or other internal magnetic interactions. Thus, the spin waves are launched by the effective magnetic field component of a laser pulse $\mathbf{h}(z,t)$, travelling in the *z*-direction, which we define as the direction normal to the sample surface. As the characteristic wavelength of the spin waves (~100 nm) is much shorter than the typical diameter of a laser spot (~ 1 μm and larger), the lateral Gaussian distribution of a laser pulse is neglected, and the excitation of the surface may be assumed to be uniform. We account for absorption of the laser pulse as it propagates from the sample boundary, resulting in an exponential spatial decay of the amplitude of the effective field $h(z,t) \sim \exp\left(-\frac{z}{d}\right)$ (see Figure 1a). Only the spin wave propagation from the first boundary is considered, as the penetration depth of the excitation is assumed to be much smaller than the sample thickness. Additionally, we assume the lifetime of the spin wave to be short enough for the spin wave to fully decay before reaching the boundary at the back of the sample. After describing the generation of propagating magnons, we also model their detection in a typical pump probe experiment, where the polarization rotation of a probe pulse induced by the dynamic magnetization is tracked as a function of time delay after excitation by the pump pulse (Figure 1b).

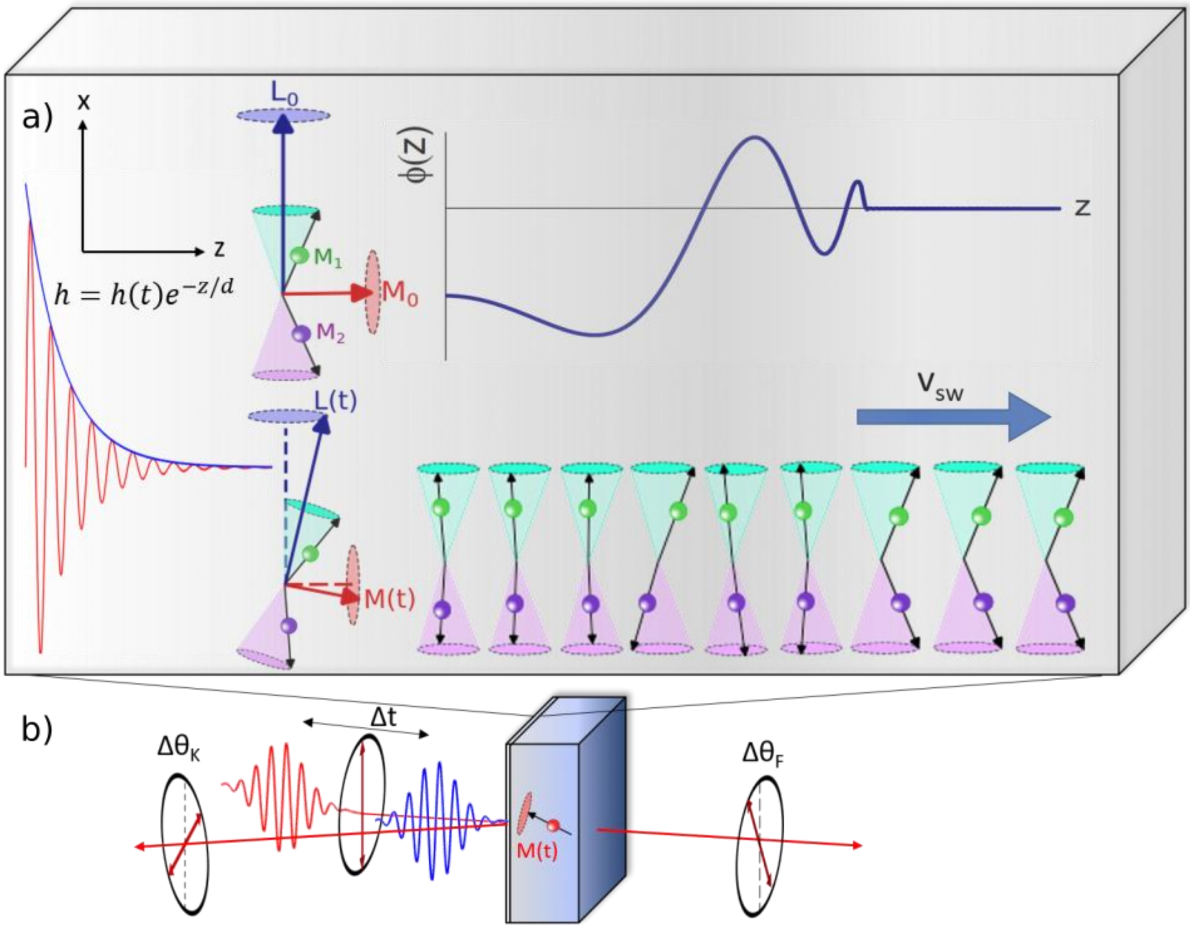

Figure 1: a) Schematic of the modelling of spin dynamics in a (canted) antiferromagnet. The spin dynamics is excited by the effective magnetic field induced by a laser pulse $h(z,t)$, which is assumed to have an exponential decay into the medium as it is absorbed. The spin excitations near the boundary propagate into the medium as waves with velocity v_{sw}. b) The spin waves are magneto-optically detected by a second laser pulse arriving after a time delay Δt. The dynamic magnetization gives rise to the Faraday rotation $\Delta\theta_F$ in the transmission configuration, or the Kerr rotation $\Delta\theta_K$ in the reflective configuration.

In antiferromagnets spin dynamics is described by the Lagrangian formalism.[48] The formalism yields two eigen-modes of antiferromagnetic resonance. As the modes are normal to each other and hence non-interacting in the linear regime, we can focus on dynamics of one of the modes (the other one is described in a similar way). In the linear regime, assuming the amplitude of the dynamic magnetization is small, the dynamics of the antiferromagnetic mode is described by the Klein-Gordon equation[49]:

$$\frac{\partial^2\varphi(z,t)}{\partial t^2} + 2\alpha\frac{\partial\varphi(z,t)}{dt} + (\omega_0^2 - c^2\nabla^2)\varphi(z,t) = -\omega_h\frac{\partial h(z,t)}{\partial t}, \tag{1}$$

where $\varphi(z,t)$ denotes the angle of deflection of the antiferromagnetic vector $L_z = L\cos\varphi, L_y = L\sin\varphi$. The damping of the precession of magnetization is given by α. The spin wave velocity limit is given by c, and $\omega_0 = \sqrt{\omega_E \omega_A}$ is the resonance frequency, which is determined by the exchange constant J ($\omega_E = \gamma L_0 J$) and anisotropy constants K_x and K_y ($\omega_A = \gamma L_0 (K_y - K_x)$), and $\omega_h = \gamma h_0$ is a parameter containing the amplitude of the effective magnetic field h_0. In these parameters, γ is the electron gyromagnetic ratio.

The spin wave dispersion relation is found by considering the plane wave solution to equation (1) in the absence of an excitation, $h(z,t) = 0$.

$$\omega^2 = \omega_0^2 + 2i\alpha\omega + c^2 {k_{\mathrm{sw}}}^2 \,. \qquad (2)$$

Here ω is the angular frequency of spin precession, k_{sw} is the wavevector of the spin wave, and c is the maximal propagation velocity of the spin wave.

We can find the solution to equation (1) analytically by performing a Fourier transformation of the equation to the frequency domain:

$$-\omega^2 \tilde{\varphi}(z,\omega) + 2i\alpha\omega\tilde{\varphi}(z,\omega) + (\omega_0^2 - c^2\nabla^2)\tilde{\varphi}(z,\omega) = -i\omega\omega_h \tilde{h}(z,\omega) \,, \qquad (3)$$

where $\tilde{\varphi}(z,\omega)$ is the Fourier transform of the spin deflection angle and $\tilde{h}(z,\omega)$ is the Fourier transform of the effective magnetic field. Only those pulse profiles are considered here, which can be written as a product of time- and space-dependent functions that, as we show below, describe the most typical excitation mechanisms. The spatial dependence is defined by the absorption of the pulse, resulting in an exponential decay, such that the magnetic field excitation in the frequency domain can be written as

$$\tilde{h}(z,\omega) = \tilde{H}(\omega)\exp(-\frac{z}{d}) \,. \qquad (4)$$

Here d is the penetration depth of the laser excitation. We assume here that the spin waves propagate unidirectionally (since the lateral size of the laser spot is much larger than all other characteristic dimensions), along the direction of the propagation of the laser pulse. The full solution for the spin deflection is then given by

$$\tilde{\varphi}(z,\omega) = f(\omega)\exp(-ik_{\mathrm{sw}}(\omega)z) + p(\omega)\exp(-\frac{z}{d}) \,. \qquad (5)$$

The first term corresponds to the solution for freely propagating magnons, where $f(\omega)$ is the spectral amplitude of the freely propagating waves and $k_{\mathrm{sw}}(\omega)$ is the wavevector determined by the dispersion relation (2). Its value is complex, with the imaginary part being responsible for the spatial decay of the spin wave. The value of k_{sw} is therefore defined as $k_{\mathrm{sw}} = \kappa - i\eta$, where κ and η are real. The second term in equation (5) corresponds to the forced solution of spin precession driven by the effective magnetic field of the laser pulse. The spectral amplitude $p(\omega)$ of this driven spin precession is directly obtained from equation (3):

$$p(\omega) = \frac{-i\omega\omega_h \widetilde{H}(\omega)}{-\omega^2 + \omega_0^2 + 2i\alpha\omega - \frac{c^2}{d^2}}. \tag{6}$$

To determine the amplitude of the freely propagating spin wave, it is required to specify the boundary conditions. The exchange boundary condition is applied here, which in its general form reads[50]

$$\frac{\partial\varphi}{\partial z}(z = 0) + \xi\varphi(z = 0) = 0\,, \tag{7}$$

where ξ is a pinning parameter determining how strongly the spins are pinned to the surface. In the case of $\xi=0$, spin deflections can occur freely at the boundary whereas for $\xi \rightarrow \infty$, spin deflections at the boundary are forbidden. Applying these boundary conditions to expression (5) allows us to determine the relation between the amplitude of the free and forced solutions:

$$f(\omega) = p(\omega)\frac{\frac{1}{d} - \xi}{\xi - ik_{\mathrm{sw}}(\omega)}\,. \tag{8}$$

Finally, one can apply inverse Fourier transformed numerically to equation (5) in order to obtain the evolution of the spin wave in the time domain. We perform this calculation for several indicative effective magnetic field profiles, which will be separately discussed in the following sections.

III. Spin wave generation results

A. Impulsive excitation

The simplest case to be considered is the impulsive excitation, where the laser pulse is modelled to be infinitesimally short in time: $h(t) = \tau h_0 \delta(t)$, where the typical laser pulse duration $\tau = 0.1$ ps is used to normalize the Dirac-delta function. This approximation describes well typical experiments with femtosecond pump pulses acting as opto-magnetic fields, which are much shorter than the period of antiferromagnetic modes. Performing the Fourier transform of the effective field $h(t)$ we obtain for the driven solution:

$$p(\omega) = \frac{-i\omega\tau\sqrt{\pi}\omega_h}{-\omega^2 + \omega_0^2 + 2i\alpha\omega - \frac{c^2}{d^2}}\,. \tag{9}$$

In the simulation, we choose the following set of parameters: $\omega_0 = 0.15$ THz, $\alpha = 10^{-2}\omega_0$, $d = 50$ nm, $c = 20$ nm/ps.[49] The results of the simulations for perfectly pinned spins are shown in Figure 2a (see also Supplementary movie 1 [51]). In Figure 2b (Supplementary movie 2 [52]), the results for the completely free boundary condition are shown. The main panels show snapshots of the evolution of the spin waves at various time points, as obtained by the numerical inverse Fourier transform of equation (5). The plots are normalized to the maximum (absolute) value of the magnetization of the snapshot at $t = 1$ ps. In the insets, the spectra are shown at a point of $z = 0.2$ μm from the boundary. We notice that the spectrum in the pinned boundary condition is much wider than in the free boundary condition, giving rise to higher frequency components. This gives rise to more pronounced spin waves in the pinned boundary condition as compared to the free boundary condition.

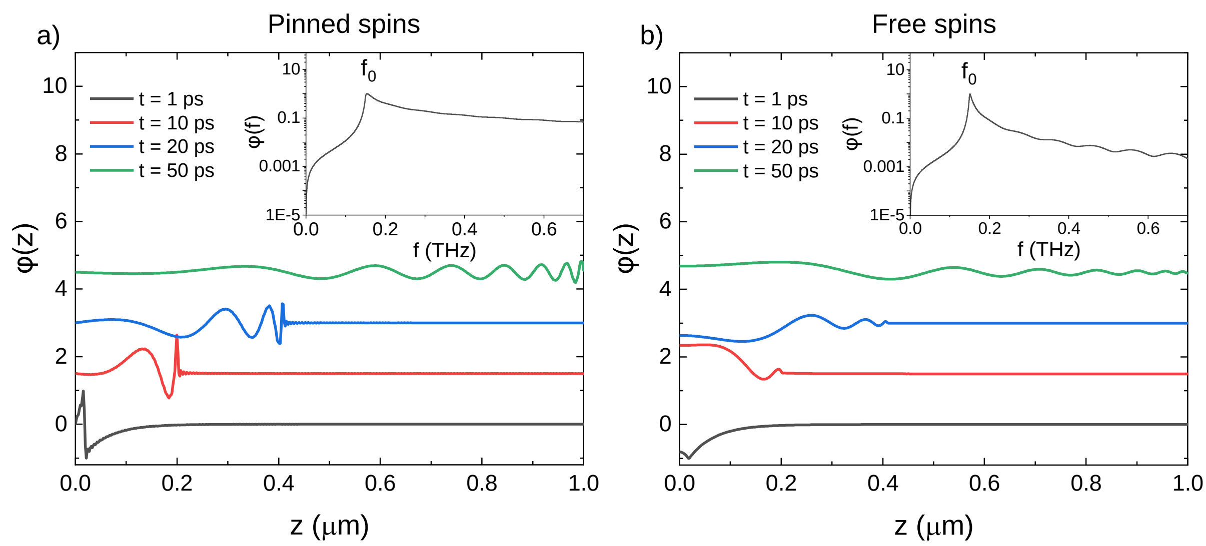

Figure 2: Snapshots of spin waves for an impulsive excitation profile. a) The spin waves at various time points for the pinned boundary condition. b) The spin waves at various time points for the free boundary condition. In both panels, the insets show the corresponding spectra at a distance z=0.2 μm from the boundary. All signals are normalised to the maximum absolute value of spin deflection at t =1 ps.

B. Displacive Excitation

The next pulse profile we consider corresponds to the displacive excitation, where the spin deflection is continuously excited, but the excitation amplitude decays over time: $h(t) = \vartheta(t)\exp(-\beta t)$, where $\vartheta(t)$ is the Heaviside step function and β is the decay parameter. This models the abrupt photoinduced change in magnetic anisotropy, which may slowly decay in time.[53] The modelling parameter values are equal to the case of impulsive excitation. We find a similar form of the forced solution as the impulsive excitation, however with a modified frequency distribution:

$$p(\omega) = \frac{-i\omega\omega_h}{(\beta+i\omega)(-\omega^2+2i\alpha\omega+\omega_0^2-\frac{c^2}{d^2})}\,. \tag{10}$$

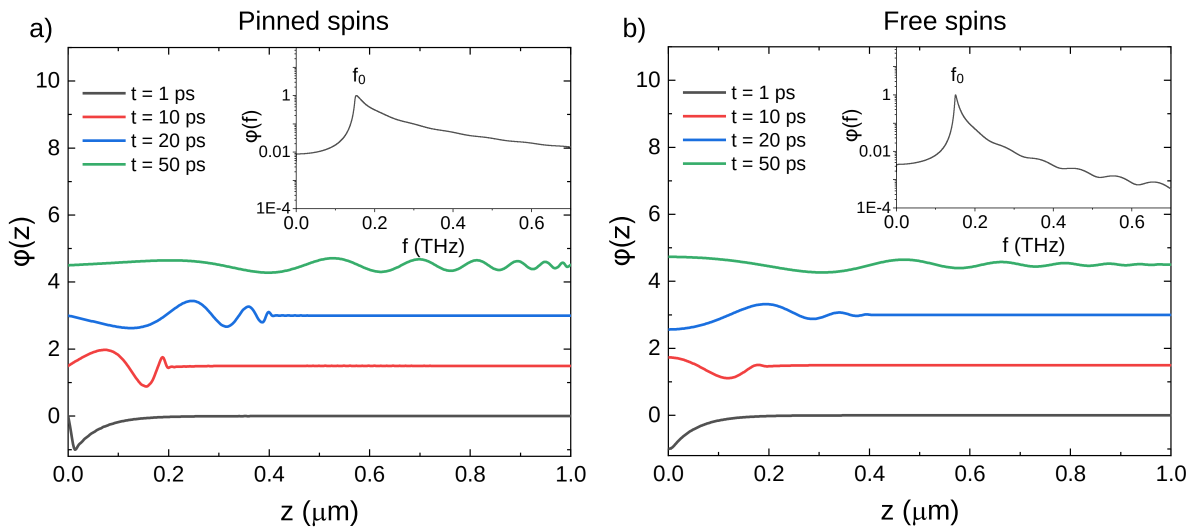

Figure 3: Snapshots of spin waves excited by a displacive excitation for a) the pinned boundary condition and b) the free boundary condition. The excitation damping parameter is $0.001\omega_0$. The insets show the corresponding spectra at a distance z=0.2 μm from the boundary. The spin waves are normalized to the maximum absolute value of the spin wave at t =1 ps.

For a value of $\beta >> \omega_0$ the decay of the excitation occurs over a much shorter time scale than a single oscillation, such that the excitation can again be approximated by a delta-function. We indeed confirmed that for such values of the lifetime of the effective field, the exact same spin wave profile is obtained as for an impulsive excitation. If $\beta << \omega_0$, the excitation decays slowly and is present over many spin oscillations. The resulting spin waves for $\beta = 0.001\omega_0$ are shown in Figure 3a (Supplementary movie 3 [54]) and Figure 3b (Supplementary movie 4 [55]) for the pinned and free boundary conditions respectively.

C. Propagating Gaussian Excitation

Finally, we consider the most general Gaussian laser pulse profile, propagating through the medium with the velocity of light $v = c_{\mathrm{opt}}/n$. Again, we account for the absorption of this pulse near the boundary. The refractive index of the medium is approximated here to be $n \approx 2.3$, typical for many antiferromagnetic oxides such as $DyFeO_3$. For the case of a propagating Gaussian pulse, some of the previously discussed equations must be modified. The propagating Gaussian profile is modelled as

$$h(z,t) = h_0 \exp(-\frac{(t-\frac{z}{v})^2}{\tau^2})\,. \tag{11}$$

The resulting solution in the Fourier domain is then given by

$$\tilde{\varphi}(\omega, z) = f(\omega)\exp(-ik_{\mathrm{sw}}z) + p(\omega)\exp\left(-\frac{z}{d}\right)\exp\left(\frac{i\omega z}{v}\right). \tag{12}$$

The relation between $f(\omega)$ and $p(\omega)$ through the boundary conditions is now slightly modified:

$$f(\omega) = p(\omega)\,\frac{\frac{1}{d} - \xi + \frac{i\omega}{v}}{\xi - ik_{\mathrm{sw}}(\omega)} \tag{13}$$

and $p(\omega)$ is now determined by the Fourier transform of the Gaussian envelope of the laser pulse:

$$p(\omega) = \frac{-i\omega\omega_h\tau\sqrt{\pi}\exp(-\omega^2\tau^2/4)}{\omega_0^2 - \omega^2 - \frac{c^2}{d^2} + 2i\alpha\omega}. \tag{14}$$

To illustrate the effect of propagation, we consider a transparent configuration in a thick sample by increasing the value of d to $d = 0.5$ cm. We take an experimentally realistic duration of the Gaussian pulse of $\tau = 100$ fs. The results of the simulation are shown in Figure 4.

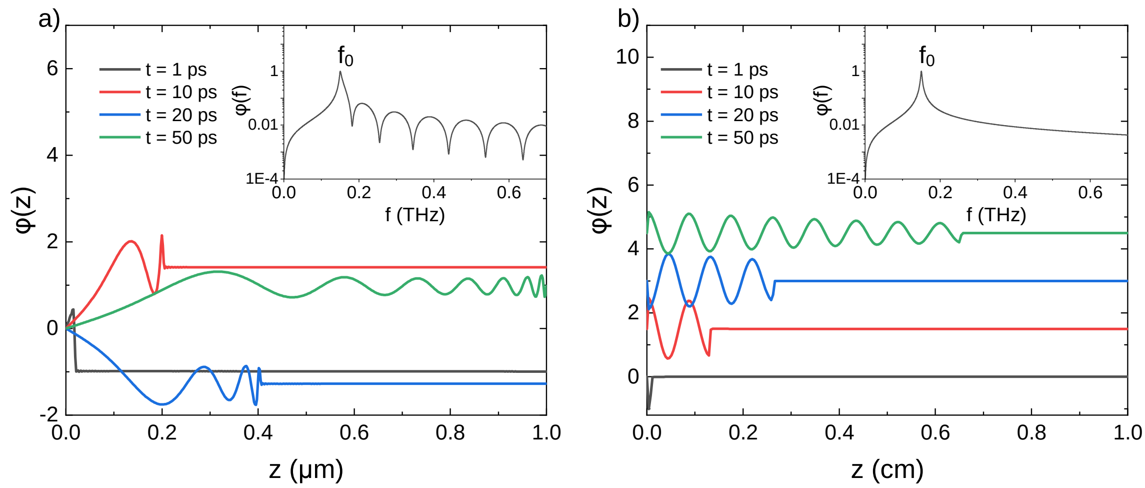

Figure 4: Snapshots of spin waves for a Gaussian propagating excitation with pinned boundary conditions on different length scales. a) The propagation of the spin wave in a micrometer range to the boundary. The inset shows the spectrum at z=0.2 µm. b) The effect of propagation of the pump pulse, driving homogeneous spin precession in the bulk on a centimeter length scale. The inset shows the spectrum at z=0.4 cm. The spin waves are normalized to the maximum absolute value of the spin wave at t =1 ps.

As the propagation of the laser pulse is much faster than the propagation of the magnon, oscillations due to the free propagation of the magnon and the driven spin precession by the effective magnetic field appear on very different length scales. Hence, in Figure 4 the solution is shown separately close to the boundary (Figure 4a, Supplementary movie 5 [56]) and in the bulk (Figure 4b, Supplementary movie 6 [57]). From these results, it is confirmed that the freely propagating spin waves only exist close to the boundary (these waves can be seen as magnonic analogue to electro-magnetic transition radiation, arising from discontinuity in the media)[58]. On the other hand, the forced oscillations only appear on long length scales and are negligible close to the boundary. However, in the transmission pump probe experiments the forced oscillations in the bulk dominate the measured response. Hence, in most experiments to date the spin oscillations with the zero wavenumber were reported.

We note that in the absorptive configuration ($d = 50$ nm), we retrieve the spin wave profiles shown in Figure 2 for the impulsive excitation. Hence, we conclude that an experimentally realistic Gaussian laser pulse can be well approximated to act as an instantaneous impulsive excitation.

D. Effect of various parameters

In this section, the effect of various parameters is investigated. The impulsive excitation is considered here, for various values of d, c, and ξ. In addition, spin waves are shown for various values of the excitation lifetime parameter β for the case of the displacive excitation.

The spin waves for various values of these parameters are compared in Figure 5.

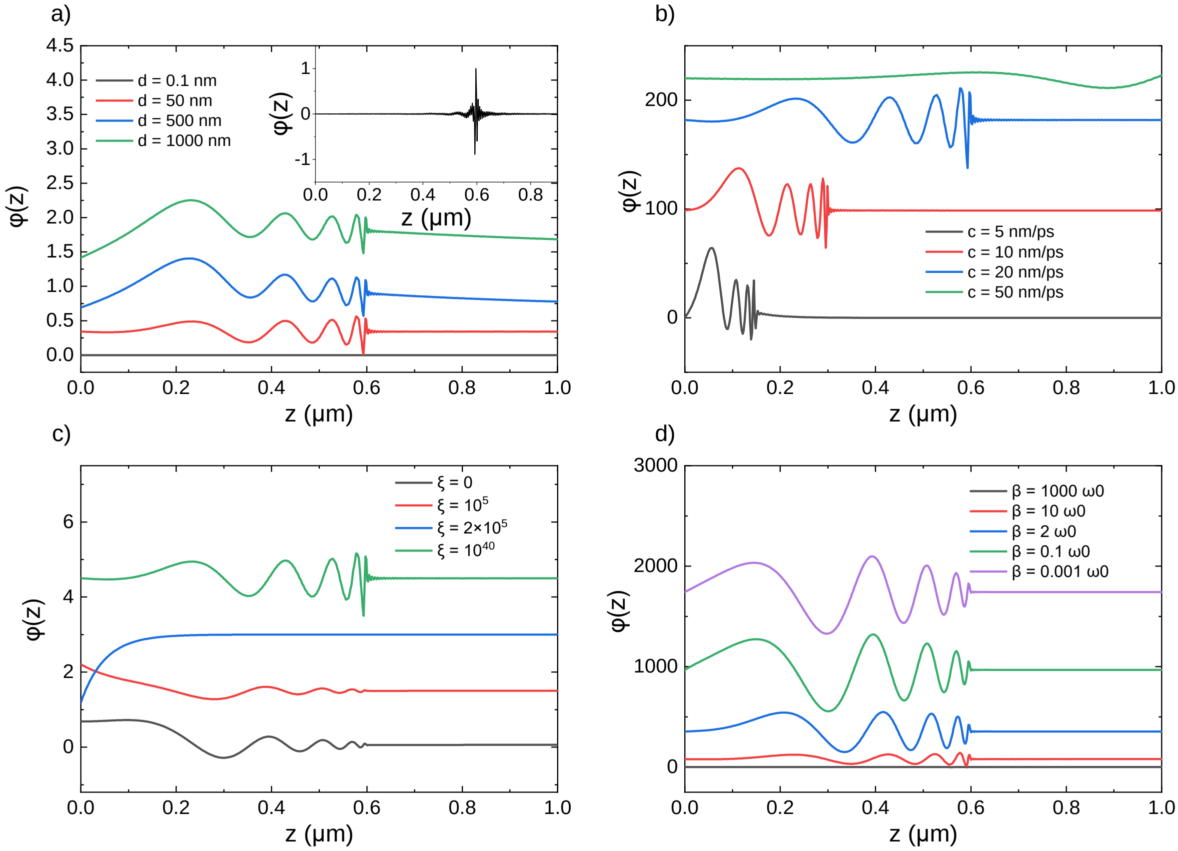

Figure 5: Spin waves under variation of several parameters: a) Variation of the optical excitation depth *d*. The inset shows a zoom-in of the spin wave for *d*=0.1 nm. b) Variation of the spin wave velocity limit *c*. c) Variation of the pinning parameter *ξ*. d) Variation of the optical excitation decay parameter *β*, for the case of the displacive excitation. Spin waves are shown at time delay *t*=30 ps.

These figures confirm expectations about the behavior of magnons. Firstly, we see in Figure 5a that confinement of the excitation to the boundary affects the profile in the spin wave, as for reducing values of *d*, the exponential decay arising from the driven precession disappears, and a stronger contribution of the freely propagating spin waves from the boundary emerges. In the limit of $d \ll \lambda_{sw}$, we see that the contribution of the driven spin precession disappears, and only the freely propagating wave remains. As the reduction in excitation depth also results in a diminished amplitude, the inset shows the normalized result for the magnon for the excitation depth of $d = 0.1$ nm. Secondly, from Figure 5b we see expected behavior when changing the velocity of the spin wave: a higher velocity results in further propagation of the spin wave from the boundary. Thirdly, in Figure 5c the effect of the pinning parameter is shown. From this one can see that the spin wave profile depends on the pinning parameter. For free boundary conditions ($\xi = 0$) spins can precess freely at $z = 0$, whereas in the limit of the perfectly pinned boundary condition ($\xi \to \infty$, approximated in our numerical code as

$\xi = 10^{40}$) precession there is restricted. We see that the ratio of the amplitudes of the propagating wavepacket and the driven spin precession depends on the pinning parameter. When the pinning parameter equals the inverse of the penetration depth, $\xi = 1/d$, (in the simulation, $\xi = 2 \times 10^5$ cm^{-1} and $d = 50$ nm), no propagating wavepacket is observed. This is directly explained by equation (8), where the amplitude of the freely propagating solution is completely suppressed. Finally, in Figure 5d we see that wavelength and amplitude of the magnon depend on the lifetime parameter of the displacive excitation β. For larger values of β, i.e. shorter excitation lifetimes, the spin wave amplitude is strongly diminished, and the central wavelength increases slightly.

E. Excitation at infinitesimal region near the boundary

As our interest is primarily on the spin waves propagating from the boundary of the material, and we have seen that the width of an experimentally realistic Gaussian laser pulse can be neglected, we now model the excitation to be a Dirac-delta function at the boundary at $z = 0$, $h(z,t) = \delta(z)\delta(t)$. This ensures that the driven solution of the spin wave is non-existent except at $z = 0$ and allows us to focus solely on the freely propagating wave. To couple the driven solution at the boundary and the freely propagating spin wave, we consider slightly altered boundary condition. We assume that the spin wave is reflected at a distance δz from the boundary, such that we can write:

$$\begin{cases} \varphi(z,\omega) = A\exp(-ik_{\mathrm{sw}}z) + B\exp(ik_{\mathrm{sw}}z) & z < \delta z \\ \varphi(z,\omega) = C\exp(-ik_{\mathrm{sw}}z) & z > \delta z \end{cases}. \tag{15}$$

To find the amplitudes, we start by integrating equation (3) over an infinitesimal region around the material boundary. From this we find that $\varphi(z,\omega)$ is continuous and its derivative $\partial\varphi(z,\omega)/\partial z$ is discontinuous at the boundary, with the discontinuity determined by the amplitude of the excitation. We also apply the pinning boundary condition as given by equation (7). Finally, we take the limit $\delta z \to 0$. As a result, we find that the spin wave propagating into the material is given by

$$\varphi(z,\omega) = \frac{i\omega\omega_h\tilde{h}(\omega)}{c^2(\xi - ik_{sw})}\exp(-ik_{sw}z)\ . \tag{16}$$

Figure 6 shows the result of this simulation

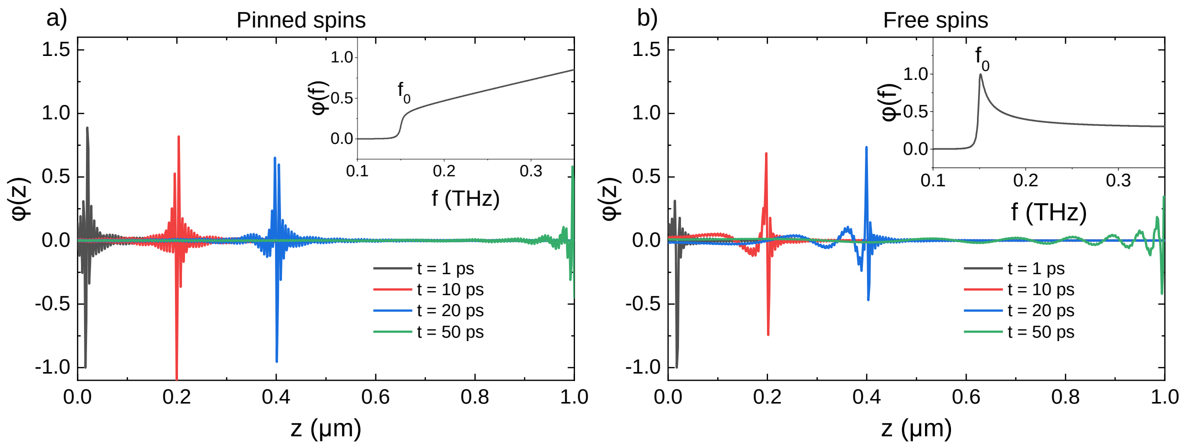

Figure 6: Snapshots of the propagating spin wave in a) the pinned boundary condition and b) the free boundary condition. The excitation exists solely at the boundary z=0 ($h(z,t)\sim\delta(z)\delta(t)$). Insets show the corresponding spectra at z=0.2 μm.

We see a large difference in the spectra for the pinned and the free boundary condition. For the pinned boundary condition, the spectral weight increases above the resonance frequency, whereas in the free boundary condition the spectral weight diminishes above the resonance frequency. As expected, we found that the results of the spin waves profiles match excellently with the case of the exponential decay considered above, for very small absorption depths of the excitation such that $d \ll \lambda_c$ (see inset Figure 5a). Thus, the waveforms shown in Figure 6 correspond to the largest k-vectors range, which can be excited by the laser pulse in the case of its strongest localization.

The situation modeled here can be realized in an antiferromagnet capped by a thin (a few nm) ferromagnetic metal layer coupled to the antiferromagnetic order via e.g. exchange bias.[59] The pump laser pulse can instantaneously heat the metal and destroy its magnetization, hence exerting a torque to the antiferromagnet at the interface. We actually believe that the modes with ‘unusual’ frequencies observed in the pump probe studies of metal-antiferromagnetic bilayers and tentatively attributed to magnetic impurities in Ref. [60] could in fact be the propagating spin waves excited at the metal-antiferromagnet interface.

IV. Model for magneto-optical detection

Spin dynamics can be detected by laser pulses with magneto-optical effects. We have shown above that the spin waves are localized in a region close to the excited boundary. Therefore, we consider a detection scheme in reflective geometry as used in the experiment in Ref. 43.

We calculate here the rotation of the plane of polarization as a result from the magneto-optical Kerr effect. This phenomenon originates from a helicity dependent refractive index in materials with broken time reversal symmetry. For simplicity, the probe pulse is assumed to be perfectly linearly polarized along the *x*-axis. The normalized incident electric field vector $\boldsymbol{e}_i$ in the (*xy*) plane can then be decomposed in circularly polarized components:

$$\mathbf{e}_i = \frac{1}{2}\mathbf{e}^+ + \frac{1}{2}\mathbf{e}^- \,, \tag{17}$$

where $\mathbf{e}^\pm = \begin{pmatrix} 1 \\ \mp i \end{pmatrix}$. Then the reflected field is:

$$\mathbf{e}_r = \frac{1}{2}r^+\mathbf{e}^+ + \frac{1}{2}r^-\mathbf{e}^- \,. \tag{18}$$

The helicity dependent reflectivity results in a small rotation of the polarization

$$\theta \approx \frac{i(r^- - r^+)}{r^- + r^+} \,. \tag{19}$$

The change in reflection coefficients originates from the presence of magnetization, affecting the refractive indices for right-handed and left-handed helicity. In a medium that has magnetization along the z-axis, two electromagnetic eigenmodes exist, with left-handed and right-handed polarization, experiencing different refractive indices. From these effective refractive indices, the effective permittivity modulation $\Delta\varepsilon$ can be obtained:[61]

$$n_\pm^2 = \varepsilon \pm g = \varepsilon + \Delta\varepsilon \,, \tag{20}$$

where g is the gyration term. Typically, this gyration term is proportional to the magnetization: $g = aM$. From this it is found that:

$$\Delta\varepsilon(z,t) = \pm aM(z,t) \,. \tag{21}$$

To find the change in reflectivity as a function of the modulation in the permittivity, we take a similar approach that was used for the ultrafast detection of acoustic phonons, in which the phonon-induced strain affects the reflectivity. We employ the following expression that was derived in Ref. [62]:

$$r = r_0 + \frac{ik_0^2}{2k} t_0 \tilde{t}_0 \int_0^\infty dz' e^{2ikz'} \Delta\varepsilon(z,t) \,. \tag{22}$$

Here, r_0 is the static reflection coefficient in the absence of a perturbation in the permittivity, t_0 is the transmission coefficient of the light into the medium and $\tilde{t}_0$ is the transmission coefficient into free space, k_0 is the wave-vector of the light in free space, and k is its wave-vector in the medium. For simplicity, we consider the case of a pure antiferromagnet, such that the difference in reflection- and transmission-coefficients and wave vectors for both helicities in statics is negligible, simplifying equation (22) to

$$r^{\pm} = r_0 \pm \Delta r \,, \tag{23}$$

where

$$\Delta r = i\,\frac{ak_0^2}{2k}\, t_0 \tilde{t}_0 \int_0^{\infty} dz' e^{2ikz'} M(z',t) \,. \tag{24}$$

For the magnetization $M(z,t)$ we use the full solution that was obtained as the inverse Fourier transform of equation (12). We note that the Kerr rotation is caused by the out of plane component of the ferromagnetic component M_z, whereas our modelled spin deflections were modelled for the antiferromagnetic L_y components. Therefore, we need to convert the previously obtained amplitudes of spin deflections of the dynamic l_y [$\mathbf{L}=\mathbf{L}_0+\mathbf{l}(t)$] component to the normal ferromagnetic spin deflection. By writing the Landau-Lifshitz equations for a two-sublattice antiferromagnet, we can relate the dynamics of the ferromagnetic m_z component to the dynamics of the antiferromagnetic l_y component.[29]

$$\frac{\partial m_z(t)}{\partial t} = \left(\omega_A - \frac{c^2}{\omega_E}\nabla^2\right) l_y(t) \,. \tag{25}$$

We can rewrite this expression in the Fourier domain to relate the spectral amplitudes of the normal ferromagnetic component to the spectral amplitudes of the antiferromagnetic component

$$\widetilde{m}_z(\omega) = \frac{1}{i\omega}\left(\omega_A - \frac{c^2}{\omega_E}\nabla^2\right) \tilde{l}_y(\omega) \,. \tag{26}$$

We employ this expression subsequently for the freely propagating part of the solution and the driven part of the solution. The obtained expressions for the dynamic magnetization is inserted in (24) and subsequently combined with equations (23) and (19). We recall that the wave-vector of the spin wave is complex and is written as $k_{\mathrm{sw}} = \kappa - i\eta$. In the case of $\eta \neq\ 0$, the spin waves decay when they are propagating away from the boundary, and the integral (24) over z converges. As a result, the following expression for the rotation angle is obtained:

$$\theta(t) = \frac{ak_0^2}{2kr_0} t_0 \tilde{t}_0 \int_{-\infty}^{\infty} d\omega e^{i\omega t}\left(f(\omega)\frac{1}{2k-k_{\mathrm{sw}}(\omega)} + p(\omega)\frac{1}{2k+i/d}\right), \tag{27}$$

with the integral over the frequency representing the Inverse Fourier Transform. Now $f(\omega)$ represents the amplitude of the m_z-component of the freely propagating spin wave and $p(\omega)$ represents the amplitude of the m_z-component of the particular solution for the magnon that is driven by the effective field. The freely propagating solution term in equation (27) has a pole for $2k = k_{sw}(\omega)$, implying a selective detection of free spin waves with wave-vectors satisfying $2k - k_{sw}(\omega) \approx 0$. If one rewrites this condition for detection in terms of wavelengths $2\lambda_{sw} = \lambda_{opt}$, the well-known Bragg condition is obtained. We can interpret the emergence of this Bragg condition by considering the propagating spin wave to effectively act as a diffraction grating due to the spatial modulation of the permittivity, enhancing reflectivity of certain wavelengths of the probe pulse.[63]

V. Results of magneto-optical spin wave detection

To illustrate how this affects the detection, we obtain the predicted spectrum of the Kerr rotation angle by evaluating the integrand in equation (27) for various wavelengths of the probe pulse. The time domain signal may then be obtained by an inverse Fourier transformation. As discussed before, the width of the Gaussian and the propagation of the pulse are negligible, so we can model the excitation to be impulsive. We model the detection of spin waves for both the pinned and free boundary condition, for an excitation depth of $d =$ 50 nm. The results are shown in Figure 7a for the pinned boundary condition and Figure 7b for the free boundary condition. The results are shown for a variety of probe wavelengths.

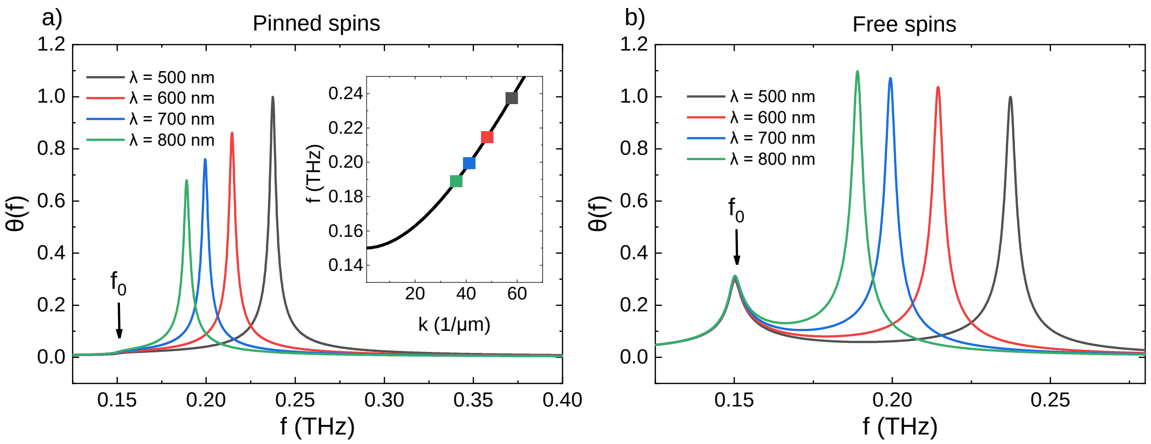

Figure 7: Spectra for an impulsive spin wave excitation as would be detected in a MOKE experiment. The spectra are calculated for multiple probe wavelengths λ. a) Calculated spectrum in the pinned boundary condition. The inset shows the dispersion relation, with the colored points indicating the selected frequency by the various probe wavelengths. b) Spectrum in the free boundary condition.

Comparison of the results in Figure 7 shows a difference in detected signal for the pinned and the free boundary conditions. The spectral amplitude at the fundamental resonance frequency of 0.15 THz disappears completely in the case of the pinned boundary condition, whereas in the free boundary condition a feature at the fundamental resonance frequency is still visible. In addition to the peak at fundamental resonance frequency, we find a second feature in the spectra at a frequency depending on the wavelength of the probe pulse. We see that with increasing photon energy, the detected spin wave is blue shifted, as a result of the Bragg condition that was imposed in equation (27). The inset in Figure 7a shows the dispersion relation. The colored points indicate the spin wave wavevectors that are probed by the optical probe pulse ($k_{\text{sw}} = 2k_{\text{opt}}$) and the matching frequencies. We see that the frequencies observed in the spectrum match the Bragg-selected frequencies in the dispersion relation. The results of our model are in excellent agreement with the experimental data reported in Ref. 43.

We also investigate the effect of the excitation localization to the boundary, by performing the simulation for various excitation depths. The results are shown in Figure 8 using both the pinned (Figure 8a) and free (Figure 8b) boundary conditions, for a probe wavelength of $\lambda =$ 800 nm.

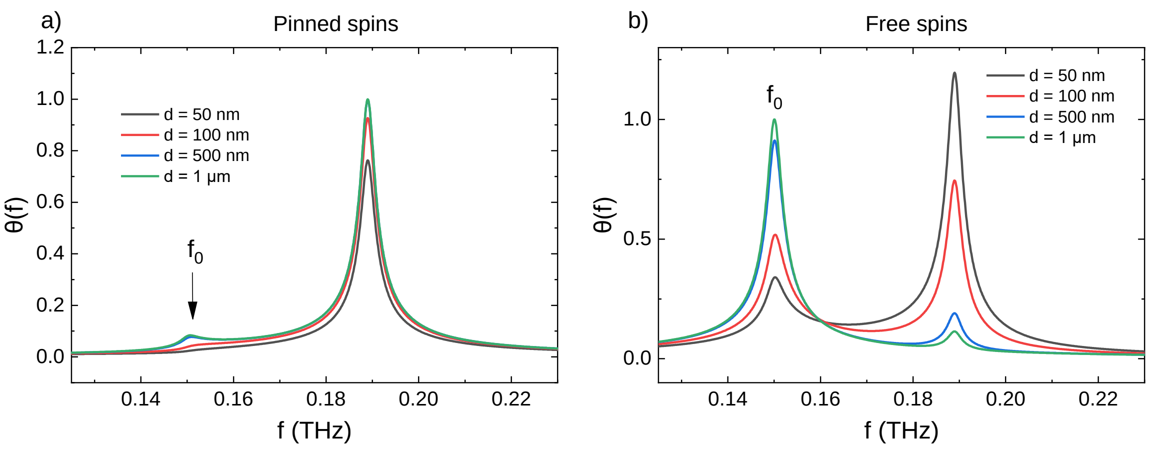

Figure 8: Spectra of the spin waves for various values of excitation depth d. a) Spectra in the pinned boundary condition. b) Spectra in the pinned boundary condition. The probe wavelength in these figures is 800 nm.

We see again the diminished spectral amplitude at the fundamental resonance frequency of 0.15 THz in the pinned boundary condition. The amplitude of the peak arising from the Bragg condition does not seem to be strongly affected by the value of the excitation depth. On the other hand, we see that the ratio of amplitudes of the two peaks are strongly dependent on the excitation depth for the free boundary condition. While the value of d increases, the contribution of the fundamental frequency is enhanced and the contribution from the Bragg reflection is reduced. As a result, for extremely short excitation depths, the detected signal will be dominated by the Bragg-selected frequencies. For long excitation depths, the detected dynamics is expected to be at the fundamental resonance frequency. For intermediate excitation depths and the free boundary condition, beating in the time domain of the signal is expected, which depends on the exact value of d. This implies that if a proper excitation depth d is chosen, the character of the boundary condition can be experimentally determined.

Finally, we investigate the effect of the pinning parameter on the detection scheme. As was already discussed before, in the case of completely pinned boundary condition, no peak at the fundamental frequency is observed. In the case of completely free spins, a dominant feature is seen at the finite k_{sw} peak, but in addition a smaller feature remains at the fundamental frequency of the k_{sw}=0 mode. As we saw before in section III.D. in the special case of $\frac{1}{d} = \xi$, the freely propagating solution is fully suppressed and as a result, only a peak at the k_{sw}=0 frequency is observed in the MOKE spectrum. For intermediate pinning parameters, when the pinning parameter is in a similar order of magnitude as the inverse penetration depth, we observe a redshift in the k_{sw}=0 peak. We understand this as the emergence of an extra pole in the detection equation (27). This additional pole appears in $f(\omega)$. As seen from equation (8) if $\xi \approx ik_{sw}(\omega)$ there will be another maximum in the detected MOKE spectrum. We confirm that the frequency at which this peak appears matches exactly with the frequency at which the imaginary part of the wavevector is equal to the pinning parameter. In our calculation, this indeed matches to the frequencies $\omega < \omega_0$. Note that the imaginary part of the spin wave wavevector arises from the fact that we calculate the magnon wavevector from the frequency through the dispersion relation (equation (2)), which has an imaginary part for $\omega < \omega_0$.

VI. Conclusions

To summarize, we have derived a model for the optical generation and detection of spin waves in an antiferromagnet. By considering different excitation profiles, among which the most general propagating Gaussian pulse, we found that for experimentally realistic parameters, the laser excitation can be appropriately modelled to be an infinitesimally short excitation. Also, we have revealed that the spin wave remains localized to the boundary, and that spin waves travel much slower than the laser excitation, so that we can neglect the propagation of the pump pulse for the generation of the spin waves. Furthermore, we have derived a formalism for the magneto-optical detection of these spin waves. In reflective pump-probe geometry we have calculated the magneto-optical Kerr effect and have shown that the spin waves are selectively detected through the arising of the Bragg condition. As a result, we have demonstrated that the detected frequency of the spin waves blue shifts for increasing probe frequency. These observations in the models can be confirmed experimentally by scanning over the probe frequency and variation of the penetration depth of the pulse, for example by varying the angle of incidence. We find that our results are in excellent agreement with a recently performed experiment of optical generation and detection of propagating magnons in an antiferromagnet.[43]

Furthermore, we have identified differences in the detection of spin waves in the pinned and free boundary conditions, implying that it should be possible to experimentally identify these boundary conditions. Further insight in the boundary conditions may provide additional information on the properties of materials, as the pinning of spins to the boundary depends on the surface anisotropy of the material and the non-uniformity of the exchange field.[50]

In conclusion, we note that the developed formalism can be easily extended to describing experiments with THz and infrared pump pulses simply by appropriate choice of the effective magnetic field profile (e.g. by digitizing the actual waveform of the THz magnetic field). We believe it will serve as a basic theoretical framework in the emerging field of antiferromagnetic magnonics, helping to guide the future experimental work. We also note that in the present model we considered only small spin deflection in the linear regime of excitation. This is thus only the first step in theoretical modeling of laser-driven magnon dynamics in antiferromagnets. The further development of the formalism will allow to include nonlinear effect by replacing linearized equation (1) with the fully nonlinear Lagrangian equation of motion.

Acknowledgments

We thank D. Afanasiev and B. Ivanov for insightful discussions. The work is supported by ERC grant 852050 MAGSHAKE.

References

1 S. Holmes, A. L. Ripple & M. A. Manheimer. Energy-Efficient Superconducting Computing-Power Budgets and Requirements. *IEEE T Appl Supercon* **23** (2013).

2 M. Madami, D. Chiuchiu, G. Carlotti & L. Gammaitoni. Fundamental energy limits in the physics of nanomagnetic binary switches. *Nano Energy* **15**, 313-320 (2015).

3 N. Jones. How to stop data centres from gobbling up the world's electricity. *Nature* **561**, 163-166 (2018).

4 V. V. Kruglyak & R. J. Hicken. Magnonics: Experiment to prove the concept. *J Magn Magn Mater* **306**, 191-194 (2006).
5 V. V. Kruglyak, S. O. Demokritov & D. Grundler. Magnonics. *J Phys D Appl Phys* **43** (2010).
6 A. V. Chumak, V. I. Vasyuchka, A. A. Serga & B. Hillebrands. Magnon spintronics. *Nat Phys* **11**, 453-461 (2015).
7 A. Barman, G. Gubbiotti, S. Ladak, A. O. Adeyeye, M. Krawczyk, J. Grafe, C. Adelmann, S. Cotofana, A. Naeemi, V. I. Vasyuchka *et al.* The 2021 Magnonics Roadmap. *J Phys-Condens Mat* **33**, 413001 (2021).
8 T. Jungwirth, X. Marti, P. Wadley & J. Wunderlich. Antiferromagnetic spintronics. *Nat Nanotechnol* **11**, 231-241 (2016).
9 P. Nemec, M. Fiebig, T. Kampfrath & A. V. Kimel. Antiferromagnetic opto-spintronics. *Nat Phys* **14**, 229-241 (2018).
10 A. V. Kimel, A. Kirilyuk, A. Tsvetkov, R. V. Pisarev & T. Rasing. Laser-induced ultrafast spin reorientation in the antiferromagnet TmFeO3. *Nature* **429**, 850-853 (2004).
11 A. V. Kimel, A. Kirilyuk, P. A. Usachev, R. V. Pisarev, A. M. Balbashov & T. Rasing. Ultrafast non-thermal control of magnetization by instantaneous photomagnetic pulses. *Nature* **435**, 655-657 (2005).
12 A. V. Kimel, C. D. Stanciu, P. A. Usachev, R. V. Pisarev, V. N. Gridnev, A. Kirilyuk & T. Rasing. Optical excitation of antiferromagnetic resonance in TmFeO3. *Phys Rev B* **74** (2006).
13 J. A. de Jong, A. V. Kimel, R. V. Pisarev, A. Kirilyuk & T. Rasing. Laser-induced ultrafast spin dynamics in ErFeO3. *Phys Rev B* **84** (2011).
14 A. M. Kalashnikova, A. V. Kimel, R. V. Pisarev, V. N. Gridnev, A. Kirilyuk & T. Rasing. Impulsive generation of coherent magnons by linearly polarized light in the easy-plane antiferromagnet FeBO3. *Phys Rev Lett* **99** (2007).
15 A. M. Kalashnikova, A. V. Kimel, R. V. Pisarev, V. N. Gridnev, P. A. Usachev, A. Kirilyuk & T. Rasing. Impulsive excitation of coherent magnons and phonons by subpicosecond laser pulses in the weak ferromagnet FeBO3. *Phys Rev B* **78** (2008).
16 V. N. Gridnev. Phenomenological theory for coherent magnon generation through impulsive stimulated Raman scattering. *Phys Rev B* **77** (2008).
17 K. Yamaguchi, M. Nakajima & T. Suemoto. Coherent Control of Spin Precession Motion with Impulsive Magnetic Fields of Half-Cycle Terahertz Radiation. *Phys Rev Lett* **105** (2010).
18 T. Kampfrath, A. Sell, G. Klatt, A. Pashkin, S. Mahrlein, T. Dekorsy, M. Wolf, M. Fiebig, A. Leitenstorfer & R. Huber. Coherent terahertz control of antiferromagnetic spin waves. *Nat Photonics* **5**, 31-34 (2011).
19 S. Baierl, M. Hohenleutner, T. Kampfrath, A. K. Zvezdin, A. V. Kimel, R. Huber & R. V. Mikhaylovskiy. Nonlinear spin control by terahertz-driven anisotropy fields. *Nat Photonics* **10**, 715-718 (2016).
20 M. van Kampen, C. Jozsa, J. T. Kohlhepp, P. LeClair, L. Lagae, W. J. M. de Jonge & B. Koopmans. All-optical probe of coherent spin waves. *Phys Rev Lett* **88** (2002).
21 T. Satoh, R. Iida, T. Higuchi, M. Fiebig & T. Shimura. Writing and reading of an arbitrary optical polarization state in an antiferromagnet. *Nat Photonics* **9**, 25-29 (2015).
22 V. Saidl, P. Nemec, P. Wadley, V. Hills, R. P. Campion, V. Novak, K. W. Edmonds, F. Maccherozzi, S. S. Dhesi, B. L. Gallagher *et al.* Optical determination of the Neel vector in a CuMnAs thin-film antiferromagnet. *Nat Photonics* **11**, 91-96 (2017).
23 J. Nishitani, K. Kozuki, T. Nagashima & M. Hangyo. Terahertz radiation from coherent antiferromagnetic magnons excited by femtosecond laser pulses. *Appl Phys Lett* **96** (2010).
24 T. Higuchi, N. Kanda, H. Tamaru & M. Kuwata-Gonokami. Selection Rules for Light-Induced Magnetization of a Crystal with Threefold Symmetry: The Case of Antiferromagnetic NiO. *Phys Rev Lett* **106** (2011).
25 N. Kanda, T. Higuchi, H. Shimizu, K. Konishi, K. Yoshioka & M. Kuwata-Gonokami. The vectorial control of magnetization by light. *Nat Commun* **2** (2011).

26 J. Nishitani, T. Nagashima & M. Hangyo. Coherent control of terahertz radiation from antiferromagnetic magnons in NiO excited by optical laser pulses. *Phys Rev B* **85** (2012).

27 J. Nishitani, T. Nagashima & M. Hangyo. Terahertz radiation from antiferromagnetic MnO excited by optical laser pulses. *Appl Phys Lett* **103** (2013).

28 R. V. Mikhaylovskiy, E. Hendry, V. V. Kruglyak, R. V. Pisarev, T. Rasing & A. V. Kimel. Terahertz emission spectroscopy of laser-induced spin dynamics in TmFeO3 and ErFeO3 orthoferrites. *Phys Rev B* **90**, 184405 (2014).

29 R. V. Mikhaylovskiy, E. Hendry, A. Secchi, J. H. Mentink, M. Eckstein, A. Wu, R. V. Pisarev, V. V. Kruglyak, M. I. Katsnelson, T. Rasing *et al.* Ultrafast optical modification of exchange interactions in iron oxides. *Nat Commun* **6**, 8190 (2015).

30 P. Sivarajah, A. Steinbacher, B. Dastrup, J. Lu, M. L. Xiang, W. Ren, S. Kamba, S. X. Cao & K. A. Nelson. THz-frequency magnon-phonon-polaritons in the collective strong-coupling regime. *J Appl Phys* **125** (2019).

31 K. Grishunin, T. Huisman, G. Q. Li, E. Mishina, T. Rasing, A. V. Kimel, K. L. Zhang, Z. M. Jin, S. X. Cao, W. Ren *et al.* Terahertz Magnon-Polaritons in TmFeO3. *Acs Photonics* **5**, 1375-1380 (2018).

32 R. V. Mikhaylovskiy, E. Hendry & V. V. Kruglyak. Negative permeability due to exchange spin-wave resonances in thin magnetic films with surface pinning. *Phys Rev B* **82** (2010).

33 I. Razdolski, A. Alekhin, N. Ilin, J. P. Meyburg, V. Roddatis, D. Diesing, U. Bovensiepen & A. Melnikov. Nanoscale interface confinement of ultrafast spin transfer torque driving non-uniform spin dynamics. *Nat Commun* **8**, 1-5 (2017).

34 M. L. M. Lalieu, R. Lavrijsen, I. R. A. Duine & B. Koopmans. Investigating optically excited terahertz standing spin waves using noncollinear magnetic bilayers. *Phys Rev B* **99** (2019).

35 D. Bossini, S. Dal Conte, Y. Hashimoto, A. Secchi, R. V. Pisarev, T. Rasing, G. Cerullo & A. V. Kimel. Macrospin dynamics in antiferromagnets triggered by sub-20 femtosecond injection of nanomagnons. *Nat Commun* **7** (2016).

36 Shubhankar Das, A. Ross, X. X. Ma, S. Becker, C. Schmitt, F. Van Duijn, E. F. Galindez-Ruales, F. Fuhrmann, M. A. Syskaki, U. Ebels *et al.* Anisotropic long-range spin transport in canted antiferromagnetic orthoferrite YFeO3. *Nat Commun* **13**, 6140 (2022).

37 R. Lebrun, A. Ross, S. A. Bender, A. Qaiumzadeh, L. Baldrati, J. Cramer, A. Brataas, R. A. Duine & M. Kläui. Tunable long-distance spin transport in a crystalline antiferromagnetic iron oxide. *Nature* **561**, 222-225 (2018).

38 R. Lebrun, A. Ross, O. Gomonay, V. Baltz, U. Ebels, A. L. Barra, A. Qaiumzadeh, A. Brataas, J. Sinova & M. Kläui. Long-distance spin-transport across the Morin phase transition up to room temperature in ultra-low damping single crystals of the antiferromagnet α-Fe2O3. *Nat Commun* **11**, 6332 (2020).

39 Maciej Dąbrowski, Takafumi Nakano, David M. Burn, Andreas Frisk, David G. Newman, Christoph Klewe, Qian Li, Mengmeng Yang, Padraic Shafer, Elke Arenholz *et al.* Coherent Transfer of Spin Angular Momentum by Evanescent Spin Waves within Antiferromagnetic NiO. *Phys Rev Lett* **124**, 217201 (2020).

40 T. Satoh, Y. Terui, R. Moriya, B. A. Ivanov, K. Ando, E. Saitoh, T. Shimura & K. Kuroda. Directional control of spin-wave emission by spatially shaped light. *Nat Photonics* **6**, 662-666 (2012).

41 Y. Au, M. Dvornik, T. Davison, E. Ahmad, P. S. Keatley, A. Vansteenkiste, B. Van Waeyenberge & V. V. Kruglyak. Direct Excitation of Propagating Spin Waves by Focused Ultrashort Optical Pulses. *Phys Rev Lett* **110** (2013).

42 A. A. Kolosvetov, M. A. Kozhaev, I. V. Savochkin, V. I. Belotelov & A. I. Chernov. Concept of the Optomagnonic Logic Operation. *Phys Rev Appl* **18**, 054038 (2022).

43 J. R. Hortensius, D. Afanasiev, M. Matthiesen, R. Leenders, R. Citro, A. V. Kimel, R. V. Mikhaylovskiy, B. A. Ivanov & A. D. Caviglia. Coherent spin-wave transport in an antiferromagnet. *Nat Phys* **17**, 1001-1006 (2021).

44 A. Stupakiewicz, A. Maziewski, I. Davidenko & V. Zablotskii. Light-induced magnetic anisotropy in Co-doped garnet films. *Phys Rev B* **64** (2001).

45 S. Kobayashi, Y. Hashimoto & H. Munekata. Investigation of an effective anisotropy field involved in photoinduced precession of magnetization in (Ga,Mn)As. *J Appl Phys* **105** (2009).

46 J. H. Mentink. Manipulating magnetism by ultrafast control of the exchange interaction. *J Phys-Condens Mat* **29** (2017).

47 R. R. Subkhangulov, A. B. Henriques, P. H. O. Rappl, E. Abramof, T. Rasing & A. V. Kimel. All-optical manipulation and probing of the d-f exchange interaction in EuTe. *Sci Rep-Uk* **4** (2014).

48 B. A. Ivanov. Spin dynamics of antiferromagnets under action of femtosecond laser pulses (Review Article). *Low Temp Phys* **40**, 91-105 (2014).

49 A. K. Zvezdin. Dynamics of Domain-Walls in Weak Ferromagnets. *Jetp Lett* **29**, 553-557 (1979).

50 A. G. Gurevich & G. A. Melkov. *Magnetization oscillations and waves*. (CRC press, 1996).

51 See Supplementary Material at [URL] for a movie of the propagation of the spin wave packet for the pinned boundary condition and an impulsive excitation.

52 See Supplementary Material at [URL] for a movie of the propagation of the spin wave packet for the free boundary condition and an impulsive excitation.

53 PI Gerevenkov, DV Kuntu, Ia A Filatov, LA Shelukhin, M Wang, DP Pattnaik, AW Rushforth, AM Kalashnikova & NE Khokhlov. Effect of magnetic anisotropy relaxation on laser-induced magnetization precession in thin galfenol films. *Physical Review Materials* **5**, 094407 (2021).

54 See Supplementary Material at [URL] for a movie of the propagation of the spin wave packet for the pinned boundary condition and a displacive excitation.

55 See Supplementary Material at [URL] for a movie of the propagation of the spin wave packet for the free boundary condition and a displacive excitation.

56 See Supplementary Material at [URL] for a movie of the propagation of the spin wave packet close to the boundary for the pinned boundary condition and a propagating Gaussian excitation.

57 See Supplementary Material at [URL] for a movie of the propagation of the spin wave packet in the bulk for the pinned boundary condition and a propagating Gaussian excitation.

58 U. Happek, A. J. Sievers & E. B. Blum. Observation of Coherent Transition Radiation. *Phys Rev Lett* **67**, 2962-2965 (1991).

59 J. Nogues & I. K. Schuller. Exchange bias. *J Magn Magn Mater* **192**, 203-232 (1999).

60 J. Tang, Y. J. Ke, W. He, X. Q. Zhang, W. Zhang, N. Li, Y. S. Zhang, Y. Li & Z. H. Cheng. Ultrafast Photoinduced Multimode Antiferromagnetic Spin Dynamics in Exchange-Coupled Fe/RFeO3 (R = Er or Dy) Heterostructures. *Adv Mater* **30** (2018).

61 A. K. Zvezdin & V. A. Kotov. *Modern magnetooptics and magnetooptical materials*. (CRC Press, 1997).

62 C Thomsen, Holger T Grahn, Humphrey J Maris & Jan Tauc. Surface generation and detection of phonons by picosecond light pulses. *Phys Rev B* **34**, 4129 (1986).

63 C. W. Sandweg, M. B. Jungfleisch, V. I. Vasyuchka, A. A. Serga, P. Clausen, H. Schultheiss, B. Hillebrands, A. Kreisel & P. Kopietz. Wide-range wavevector selectivity of magnon gases in Brillouin light scattering spectroscopy. *Rev Sci Instrum* **81** (2010).